

Sublattice-sensitive Majorana modes

Di Zhu ^{1,*}, Bo-Xuan Li,^{2,3,*} and Zhongbo Yan ^{1,†}

¹*Guangdong Provincial Key Laboratory of Magnetolectric Physics and Devices, School of Physics, Sun Yat-Sen University, Guangzhou 510275, China*

²*Beijing National Laboratory for Condensed Matter Physics and Institute of Physics, Chinese Academy of Sciences, Beijing 100190, China*

³*University of Chinese Academy of Sciences, Beijing 100049, China*

 (Received 8 December 2021; revised 21 August 2022; accepted 5 December 2022; published 15 December 2022)

For two- and three-dimensional topological insulators whose unit cells consist of multiple sublattices, the boundary terminating at which type of sublattice can affect the time-reversal invariant momentum at which the Dirac points of helical boundary states are located. By incorporating a generic theory and a representative model, we reveal that this interesting property allows the realization of Majorana modes at sublattice domain walls forming on the boundary when the boundary Dirac points of the topological insulator are gapped by appropriate superconductivity in proximity. Remarkably, we find that the sensitive sublattice dependence of the Majorana modes allows their positions to be precisely manipulated by locally controlling the terminating sublattices or boundary potential. Our work reveals that the sublattice degrees of freedom commonly found in materials open a different route to realize and manipulate Majorana modes.

DOI: [10.1103/PhysRevB.106.245418](https://doi.org/10.1103/PhysRevB.106.245418)

I. INTRODUCTION

As a class of topological excitations, Majorana modes in topological superconductors (TSCs) have attracted tremendous research enthusiasm since a connection between these modes and fault-tolerant quantum computation was built [1,2]. On the road to the final application in quantum computation, it is widely believed that a milestone will be the implementation of braiding Majorana zero modes (MZMs) [3], a type of bound-state Majorana modes. Historically, as MZMs were first revealed to appear in the vortex cores of two-dimensional chiral p -wave superconductors in the topological regime [4], the initial scenario for braiding MZMs is based on the natural idea of moving and exchanging vortices [5]. Later, theorists showed that the braiding process could also be carried out in networks of one-dimensional TSC wires [6,7]. Despite being viewed as the two most promising routes, an experimental realization of either remains elusive as unequivocally detecting and controllably manipulating vortex-core or wire-end MZMs remain challenging, even though steady and remarkable progress has been witnessed in many Majorana-candidate platforms, ranging from semiconductor nanowires [8–18] and magnetic atom chains [19–21] to superconducting topological insulators [22–24] and iron-based superconductors [25–27].

In the past few years, the study of higher-order TSCs provides different perspectives for both the implementation [28–65] and manipulation of MZMs [66–68] and other propagating Majorana modes [69–82]. A unique characteristic of

higher-order TSCs is that the concomitant Majorana modes have a codimension (d_c) larger than one and their locations in real space depend on the boundary geometry. This is fundamentally distinct from conventional TSCs (also dubbed first-order TSCs) protected by internal symmetries only [83], where the Majorana modes have $d_c = 1$ and their locations do not rely on the boundary geometry as they appear everywhere on the whole boundary. Because of the freedom on the boundary, the positions of Majorana modes in a higher-order TSC are in principle allowed to move if the Majorana modes are not pinned by any crystalline symmetry [31,33]. Indeed, previous works have shown that the positions of MZMs in two-dimensional second-order TSCs can be tuned by rotating the orientation of magnetic field [49,68,84] or changing the boundary potential via electrical gating [48,67], accordingly opening other routes to manipulate and braid MZMs [85–87]. In this work, we reveal that the sublattice degrees of freedom commonly appearing in materials admit an intriguing scheme for the realization and manipulation of Majorana modes with $d_c = 2$. This scheme can be applied to systems both with and without time-reversal symmetry (TRS), and remarkably allows the positions of Majorana modes to be precisely manipulated, thus holding great promise for the detection, manipulation, and braiding of Majorana modes.

To date, there already exist many proposals for the implementation of second-order TSCs, including topological insulator (TI)/superconductor heterostructures [34–43] and their generalizations [44–48,69–74], odd-parity superconductors [49,50, 52–56], spin-orbit coupled systems with mixed pairings [57,58], etc. In this work we consider TI/superconductor heterostructures, whose implementation is already feasible in experiments [22–24], to illustrate the physics. The physical picture can be roughly described as

*These authors contributed equally to this work.

†yanzhh5@mail.sysu.edu.cn

follows. For a d -dimensional (dD) first-order TI with $d \geq 2$, although the appearance of helical states does not depend on the terminating sublattice type on the boundary [88,89], a fact, interesting but having attracted little attention, is that the terminating sublattice type can affect the time-reversal invariant momentum (TRIM) at which the Dirac points of helical boundary states are located. Interestingly, such a dependence of boundary Dirac points on sublattice terminations can affect both the magnitude and the sign of the boundary Dirac mass induced by superconductivity in proximity [90,91]. Under appropriate conditions, such a property allows the emergence of highly controllable Majorana modes at the domain walls of two distinct sublattice terminations on the same boundary. Below we first formulate the generic theory, and then demonstrate the physics via a concrete model.

II. GENERIC THEORY FROM A BOUNDARY PERSPECTIVE

Within the mean-field framework, a superconducting system can be described by a corresponding Bogoliubov–de Gennes (BdG) Hamiltonian of the form $H = \frac{1}{2} \sum_{\mathbf{k}} \Psi_{\mathbf{k}}^{\dagger} [\mathcal{H}_N(\mathbf{k}) + \mathcal{H}_{SC}(\mathbf{k})] \Psi_{\mathbf{k}}$, where $\Psi_{\mathbf{k}}$ denotes the Nambu basis, \mathcal{H}_N describes the normal state, and \mathcal{H}_{SC} describes the superconducting pairing. When \mathcal{H}_N describes a first-order topological insulator with $d \geq 2$, one knows that helical states will appear on the boundary and form $(d-1)$ -dimensional Dirac points at TRIMs of the reduced boundary Brillouin zone [88,89]. Consider a boundary with a given type of sublattice terminations; if the chemical potential is set to cross the boundary Dirac point, then the low-energy boundary Hamiltonian will take the standard form [92]

$$\mathcal{H}_{\Gamma_s}(\mathbf{q}) = \sum_{i=1}^{d-1} v_i q_i \gamma_i, \quad (1)$$

where Γ_s denotes the TRIM at which the boundary Dirac point is located, \mathbf{q} is the momentum measured from Γ_s , v_i is the velocity along the i th direction, and the γ_i matrices satisfy the Clifford algebra, i.e., $\{\gamma_i, \gamma_j\} = 2\delta_{ij}$. The effect from the superconducting pairing to the helical states can be determined by projecting \mathcal{H}_{SC} onto the subspace spanned by the orthogonal wave functions of helical boundary states. In general, if one only considers the leading-order contribution, what the superconducting pairing induces is a constant Dirac mass term that gaps out the Dirac point. Accordingly, the low-energy physics on the boundary is described by a massive Dirac Hamiltonian of the form

$$\tilde{\mathcal{H}}_{\Gamma_s}(\mathbf{q}) = \sum_{i=1}^{d-1} v_i q_i \gamma_i + m_{\Gamma_s} \gamma_d, \quad (2)$$

with $\{\gamma_d, \gamma_{i=1, \dots, d-1}\} = 0$ and m_{Γ_s} representing the induced Dirac mass. Mathematically, the Dirac mass term is given by

$$[m_{\Gamma_s} \gamma_d]_{\alpha\beta} = \int dx_d \psi_{\alpha}^{\dagger}(x_d) \mathcal{H}_{SC}(-i\partial_{x_d}, \Gamma_s) \psi_{\beta}(x_d), \quad (3)$$

where $\{\psi_{\alpha}(x_d)\}$ denote the wave functions for the helical states localized at the x_d -normal boundary [93]. Focusing on the same boundary, if the boundary Dirac point changes from Γ_s to $\Gamma_{s'}$ due to a change of sublattice terminations, then the

boundary Hamiltonian will accordingly change to

$$\tilde{\mathcal{H}}_{\Gamma_{s'}}(\mathbf{q}') = \sum_{i=1}^{d-1} v'_i q'_i \gamma_i + m_{\Gamma_{s'}} \gamma_d, \quad (4)$$

where \mathbf{q}' denotes the momentum measured from $\Gamma_{s'}$. While the value of Fermi velocity for the helical states on a given boundary may change, the sign cannot change as each branch of the helical states must propagate in a fixed direction. However, the superconductivity-induced Dirac mass can change its magnitude as well as the sign if the pairing has certain momentum dependence or sublattice dependence, e.g., extended s -wave pairing, d -wave pairing, etc. Without loss of generality, let us now consider a nonuniform boundary consisting of two parts which take different sublattice terminations. For the convenience of discussion, we dub the interface separating two distinct types of sublattice terminations as *sublattice domain wall*. Assuming that the sublattice domain walls only break the translation symmetry of the given boundary in the x_{d-1} direction, the boundary Hamiltonian becomes

$$\begin{aligned} \mathcal{H}(-i\partial_{x_{d-1}}, \mathbf{q}'_{\parallel}) &= -i \frac{\gamma_{d-1}}{2} \{v_{d-1}(x_{d-1}), \partial_{x_{d-1}}\} + m(x_{d-1}) \gamma_d \\ &\quad + \sum_{i=1}^{d-2} v_i q'_i \gamma_i, \end{aligned} \quad (5)$$

where $\mathbf{q}'_{\parallel} = (q'_1, \dots, q'_{d-2})$ denotes the momentum parallel to the sublattice domain walls and $\{\dots\}$ denotes symmetrization of the operators. Notably, if m_{Γ_s} and $m_{\Gamma_{s'}}$ have opposite signs, then the Dirac mass $m(x_{d-1})$ will change sign across the sublattice domain walls. In other words, the sublattice domain walls are Dirac-mass domain walls. As a result, Majorana modes with $d_c = 2$ will emerge at the sublattice domain walls according to the Jackiw-Rebbi theory [94], corresponding to the realization of an extrinsic time-reversal invariant second-order TSC. As TRS is conserved, the resulting Majorana modes will be Majorana Kramers pairs (two MZMs related by TRS) in 2D [34,35] and propagating helical Majorana modes in 3D [69].

The above generic theory can be straightforwardly generalized to systems without TRS. Without loss of generality, let us consider that the TRS is broken by a Zeeman field. It is known that the Zeeman field can also induce a Dirac mass to the helical edge states, which will compete with the Dirac mass induced by superconductivity. Accordingly, this raises the possibility that the two sides of one sublattice domain wall are dominated by Dirac masses of different nature, thus leading to the emergence of MZMs in 2D and chiral Majorana modes in 3D [93]. It is worth noting that when TRS is broken, Majorana modes at sublattice domain walls can be realized even with conventional s -wave superconductivity [95,96], reflecting that the revealed physics is generic and feasible in current experiments. With the established generic theory in mind, below we focus on the case with TRS and consider a concrete realization to demonstrate the discussed physics.

III. MAJORANA KRAMERS PAIRS AT THE SUBLATTICE DOMAIN WALLS

Since 2D honeycomb lattices with just two types of sublattices allow a simple illustration of the essential physics, below we consider the representative Kane-Mele model to realize the first-order TI and further assume a proximity-induced spin-singlet pairing. The full Hamiltonian has the form

$$\begin{aligned}
 H = & t \sum_{\langle ij \rangle, \alpha} c_{i, \alpha}^\dagger c_{j, \alpha} + i \lambda_{\text{so}} \sum_{\langle\langle ij \rangle\rangle, \alpha, \beta} v_{ij} c_{i, \alpha}^\dagger (s^z)_{\alpha\beta} c_{j, \beta} \\
 & - \mu \sum_{i, \alpha} c_{i, \alpha}^\dagger c_{i, \alpha} + \left[\Delta_0 \sum_i c_{i, \uparrow}^\dagger c_{i, \downarrow}^\dagger + \sum_{\langle ij \rangle} \Delta_{1:ij} c_{i, \uparrow}^\dagger c_{j, \downarrow}^\dagger \right. \\
 & \left. + \sum_{\langle\langle ij \rangle\rangle} \Delta_{2:ij} c_{i, \uparrow}^\dagger c_{j, \downarrow}^\dagger + \text{H.c.} \right], \quad (6)
 \end{aligned}$$

where $\langle ij \rangle$ and $\langle\langle ij \rangle\rangle$ refer to nearest-neighbor and next-nearest-neighbor sites; $\alpha, \beta = \{\uparrow, \downarrow\}$ are spin indices; t, λ_{so} , and μ are the nearest-neighbor hopping constant, spin-orbit coupling strength, and chemical potential, respectively. The first line corresponds to the Kane-Mele model which realizes a 2D first-order TI as long as λ_{so} is nonzero [97,98]. $\Delta_0, \Delta_{1:ij}$, and $\Delta_{2:ij}$ represent the on-site, nearest-neighbor, and next-nearest-neighbor pairings, respectively. The reason to consider an extended s -wave pairing is due to the fact that when the TRS is preserved, a uniform on-site s -wave pairing cannot realize any topological superconducting phase [99]. Nevertheless, according to the generic theory, there is no constraint on the pairing type (a demonstration of the physics via d -wave pairing as well as staggered on-site s -wave pairing is provided in the Supplemental Material [93]). Without loss of generality, below we assume $\Delta_{1:ij} = \Delta_1$ and $\Delta_{2:ij} = \Delta_2$ for simplicity, corresponding to an extended s -wave pairing which preserves all crystalline symmetries of the normal-state Hamiltonian.

By a Fourier transformation to the momentum space and choosing the basis to be $\Psi_{\mathbf{k}}^\dagger = (\psi_{\mathbf{k}}^\dagger, \psi_{-\mathbf{k}}^\dagger)$ with $\psi_{\mathbf{k}}^\dagger = (c_{A, \mathbf{k}, \uparrow}^\dagger, c_{B, \mathbf{k}, \uparrow}^\dagger, c_{A, \mathbf{k}, \downarrow}^\dagger, c_{B, \mathbf{k}, \downarrow}^\dagger)$, the BdG Hamiltonian reads

$$\begin{aligned}
 \mathcal{H}(\mathbf{k}) = & t \sum_i [\cos(\mathbf{k} \cdot \mathbf{a}_i) \tau_z s_0 \sigma_x + \sin(\mathbf{k} \cdot \mathbf{a}_i) \tau_z s_0 \sigma_y] \\
 & + 2 \lambda_{\text{so}} \sum_i \sin(\mathbf{k} \cdot \mathbf{b}_i) \tau_0 s_z \sigma_z - \mu \tau_z s_0 \sigma_0 \\
 & - \Delta_1 \sum_i [\cos(\mathbf{k} \cdot \mathbf{a}_i) \tau_y s_y \sigma_x + \sin(\mathbf{k} \cdot \mathbf{a}_i) \tau_y s_y \sigma_y] \\
 & - \left[\Delta_0 + 2 \Delta_2 \sum_i \cos(\mathbf{k} \cdot \mathbf{b}_i) \right] \tau_y s_y \sigma_0, \quad (7)
 \end{aligned}$$

where the Pauli matrices τ_i, s_i , and σ_i act on the particle-hole, spin (\uparrow, \downarrow), and sublattice (A, B) degrees of freedom, respectively. The sum runs over $i = 1, 2, 3$, with the nearest-neighbor vectors $\mathbf{a}_1 = a(0, 1)$, $\mathbf{a}_2 = \frac{a}{2}(\sqrt{3}, -1)$, and $\mathbf{a}_3 = \frac{a}{2}(-\sqrt{3}, -1)$, and a being the lattice constant (below we set $a = 1$ for notational simplicity). The next-nearest-neighbor vectors $\mathbf{b}_1 = \mathbf{a}_2 - \mathbf{a}_3$, $\mathbf{b}_2 = \mathbf{a}_3 - \mathbf{a}_1$, and $\mathbf{b}_3 = \mathbf{a}_1 - \mathbf{a}_2$ [100]. The Hamiltonian has TRS (the time-reversal operator $\mathcal{T} =$

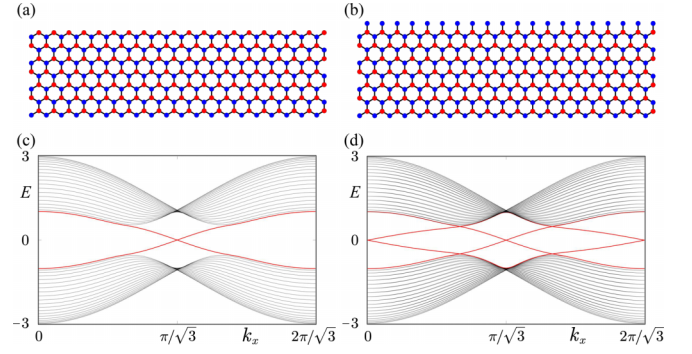


FIG. 1. Sensitivity dependence of boundary Dirac points on the terminating sublattice type. (a) The upper and lower zigzag edges of the lattice respectively terminate with sublattice B (red dots) and A (blue dots). (b) The lower edge keeps to be the same as in (a), but the upper edge changes to be a beard type, with the terminating sublattice type changing from B to A. Panels (c) and (d) show the corresponding normal-state energy spectra when the y -normal open boundaries follow the structures shown in (a) and (b), respectively. In (c) and (d), periodic boundary conditions are imposed in the x direction and parameters are $t = 1$ and $\lambda_{\text{so}} = 0.1$.

$i\tau_0 s_y \sigma_0 \mathcal{K}$ with \mathcal{K} the complex conjugate operator), particle-hole symmetry ($\mathcal{P} = \tau_x s_0 \sigma_0 \mathcal{K}$), and inversion symmetry ($I = \tau_0 s_0 \sigma_x$). Because the coexistence of TRS and inversion symmetry enforces Kramers degeneracy to the bulk bands, the first-order topology of the BdG Hamiltonian will always be trivial for the concerned spin-singlet pairing [46,74,101]. In previous works, it has been shown that a first-order TI with square lattice in proximity to an extended s -wave superconductor can realize a second-order TSC with Majorana Kramers pairs localized at the corners of a square sample [34]. Notably, therein the topological criterion requires either the hopping or the pairing to have crystalline anisotropy, because otherwise Dirac-mass domain walls cannot form on the boundary due to symmetry constraint. However, as we will show below, even though both the hopping and pairing are considered to be isotropic in Eq. (7), here Dirac-mass domain walls can emerge on the boundary due to the sublattice degrees of freedom.

For the 2D honeycomb lattice, there are two kinds of simple edges whose outermost terminations only contain one type of sublattice, which are known as zigzag and beard edges [see Figs. 1(a) and 1(b)]. Let us first investigate how the change of sublattice termination on a given boundary affects the helical edge states of the normal state. To be specific, we consider a cylindrical geometry with periodic boundary condition in the x direction and open boundary condition in the y direction. When the upper edge terminates with type-B sublattices and the lower edge terminates with type-A sublattices [see Fig. 1(a)], one finds that the boundary Dirac points for both upper and lower edges are located at $k_x = \pi/\sqrt{3}$, as shown in Fig. 1(c). By only changing the terminating sublattice type on the upper edge, one finds that one boundary Dirac point is immediately shifted from $k_x = \pi/\sqrt{3}$ to $k_x = 0$, as shown in Figs. 1(b) and 1(d). Since nothing changes in the bulk as well as on the lower edge, the shifted Dirac point apparently

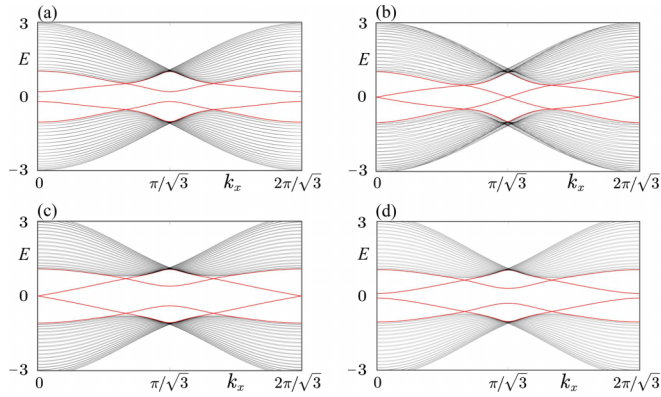


FIG. 2. Energy spectrum of the BdG Hamiltonian for a cylindrical geometry with open (periodic) boundary conditions in the $y(x)$ direction. The upper (lower) edge in the y direction is chosen to be the beard (zigzag) type. In (a)–(d), $t = 1$, $\lambda_{so} = 0.1$, $\mu = 0$, and pairing amplitudes are as follows: (a) $\Delta_0 = 0.2$, $\Delta_1 = \Delta_2 = 0$; (b) $\Delta_1 = 0.2$, $\Delta_0 = \Delta_2 = 0$; (c) $\Delta_2 = 0.2$, $\Delta_0 = \Delta_1 = 0$; (d) $\Delta_0 = 0.1$, $\Delta_1 = 0$, $\Delta_2 = 0.2$.

corresponds to the upper edge, confirming the sensitive sublattice dependence of boundary Dirac points.

Taking the superconductivity into account, numerical results show that the on-site pairing, nearest-neighbor pairing, and next-nearest-neighbor pairing have rather different effects on the helical edge states, as shown in Fig. 2. The on-site pairing, as expected, will induce a Dirac mass to gap out the Dirac points, irrespective of whether the edge is zigzag type or beard type, as shown in Fig. 2(a). In sharp contrast, Fig. 2(b) shows that the boundary Dirac points are intact to the nearest-neighbor pairing. Lastly, the next-nearest-neighbor pairing turns out to open a gap for the Dirac point of the zigzag edge but not for that of the beard edge, as shown in Fig. 2(c). These results indicate when both Δ_0 and Δ_2 are finite, the gaps opened for the Dirac points at $k_x = 0$ and $k_x = \pi/\sqrt{3}$ can be different, as shown in Fig. 2(d).

As the effect of nearest-neighbor pairing on the helical edge states is negligible, below we set $\Delta_1 = 0$ for simplicity. To obtain the topological criterion for the emergence of domain walls binding Majorana modes, we follow the generic theory and derive the low-energy boundary Hamiltonians for both zigzag and beard edges [93]. Focusing on the upper y -normal boundary and considering the case with $\mu = 0$ for illustration, we find that the boundary Hamiltonian for the beard-type edge (terminating with type-A sublattices) is

$$\mathcal{H}_{u,\text{beard}}(q_x) = vq_x\tau_0s_z - \Delta_0\tau_ys_y, \quad (8)$$

where the subscript “u” stands for “upper edge,” $v = 3\sqrt{3}\lambda_{so}$, and q_x is measured from $k_x = 0$. The boundary Hamiltonian for the zigzag-type edge (terminating with type-B sublattices) is

$$\mathcal{H}_{u,\text{zigzag}}(q'_x) = v'q'_x\tau_0s_z + (2\Delta_2 - \Delta_0)\tau_ys_y, \quad (9)$$

where $v' \approx 6\sqrt{3}\lambda_{so}$ if $\lambda_{so}/t \ll 1$ and q'_x is measured from $k_x = \pi/\sqrt{3}$ [93]. It is easy to find that the Dirac masses in the two Hamiltonians will take opposite signs if $|\Delta_2| > |\Delta_0|/2 > 0$. This is the topological criterion for sublattice domain walls

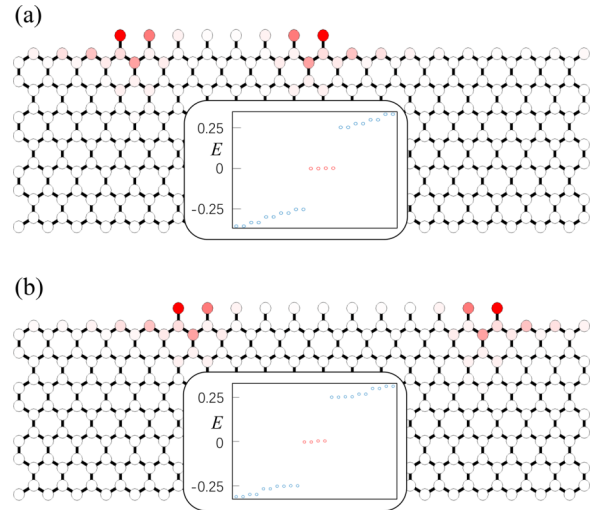


FIG. 3. Majorana Kramer pairs bounded at sublattice domain walls. Chosen parameters are $t = 1$, $\lambda_{so} = 0.1$, $\mu = 0$, $\Delta_0 = \Delta_2 = 0.3$, and $\Delta_1 = 0$. With periodic boundary conditions in the x direction except for the uppermost beard-type part, the two insets in (a) and (b) show the corresponding energy spectra. The four dots highlighted by red indicate the existence of two Majorana Kramer pairs. The shade of the red color on the lattice sites reflects the weight of the probability density of Majorana Kramer pairs.

to host Majorana Kramer pairs at $\mu = 0$. Due to the robustness of topology, this topological criterion will hold as long as μ is lower than the critical value at which the boundary energy gap gets closed [93].

To validate the established topological criterion, we again consider a cylindrical geometry with periodic boundary condition in the x direction and only let the upper edge be nonuniform, where one part terminates with B-type sublattices (zigzag) and the other part terminates with A-type sublattices (beard). Accordingly, there are two sublattice domain walls on the upper edge, while the lower edge remains uniform. As shown in Fig. 3, when the topological criterion is fulfilled, a diagonalization of the real-space Hamiltonian shows the existence of four MZMs, corresponding to two Majorana Kramer pairs. As expected, the wave functions of Majorana Kramer pairs are strongly localized around the sublattice domain walls. In addition, comparing Fig. 3(a) with Fig. 3(b), it is readily seen that the positions of Majorana Kramer pairs directly follow the change of the positions of sublattice domain walls, indicating that the positions of Majorana Kramer pairs can be adjusted site by site by a precise control of the terminating sublattices. Remarkably, even when the positions of sublattice domain walls are fixed, we find that the same goal can also be achieved by electrically tuning the local boundary potential [93].

As a final remark, it is worth mentioning that, because of the protection from particle-hole symmetry, the Majorana Kramer pairs at the sublattice domain walls are stable against time-reversal invariant disorders, e.g., random chemical potential or boundary imperfections, as long as the strength of the disorder is below the threshold [34]. Moreover, as our theory is based on helical boundary states whose robustness

is protected by TRS, the predicted physics is also expected to be at least robust against weak interactions.

IV. DISCUSSION AND CONCLUSION

While our theory is exemplified in terms of the 2D honeycomb lattice, its generality admits a wide application as sublattice degrees of freedom are ubiquitous in materials, e.g., materials with kagome lattice [95], Lieb lattice [102,103] (a study of the Lieb lattice is provided in the Supplemental Material [93]), etc. Besides quantum materials, another potential approach to realize our proposal is to create artificial lattices on the surface of superconductors [104], just like these experiments which deposited magnetic atom chains on a superconductor to realize 1D topological superconductivity [19–21]. As a different scheme for the implementation of extrinsic second-order TSCs and Majorana

modes, one remarkable advantage is that the sensitive sublattice dependence allows the positions of Majorana modes to be manipulated in a highly controllable and precise way. For experimental realization, we suggest the use of scanning tunneling/force microscopy to manipulate the sublattice terminations [105,106] and detect the comoving Majorana modes.

ACKNOWLEDGMENTS

We thank Z. Wu, M. Kheirkhah, Z. Wang, Z. Wang, and D. Zhong for helpful discussions. This work is supported by the National Natural Science Foundation of China (Grants No. 11904417 and No. 12174455) and the Natural Science Foundation of Guangdong Province (Grant No. 2021B1515020026).

-
- [1] A. Yu. Kitaev, Fault-tolerant quantum computation by anyons, *Ann. Phys. (NY)* **303**, 2 (2003).
 - [2] C. Nayak, S. H. Simon, A. Stern, M. Freedman, and S. Das Sarma, Non-Abelian anyons and topological quantum computation, *Rev. Mod. Phys.* **80**, 1083 (2008).
 - [3] S. Das Sarma, M. Freedman, and C. Nayak, Majorana zero modes and topological quantum computation, *npj Quantum Inf.* **1**, 15001 (2015).
 - [4] N. Read and D. Green, Paired states of fermions in two dimensions with breaking of parity and time-reversal symmetries and the fractional quantum Hall effect, *Phys. Rev. B* **61**, 10267 (2000).
 - [5] D. A. Ivanov, Non-Abelian Statistics of Half-Quantum Vortices in p -Wave Superconductors, *Phys. Rev. Lett.* **86**, 268 (2001).
 - [6] J. Alicea, Y. Oreg, G. Refael, F. von Oppen, and M. P. A. Fisher, Non-abelian statistics and topological quantum information processing in 1D wire networks, *Nat. Phys.* **7**, 412 (2011).
 - [7] D. Aasen, M. Hell, R. V. Mishmash, A. Higginbotham, J. Danon, M. Leijnse, T. S. Jespersen, J. A. Folk, C. M. Marcus, K. Flensberg, and J. Alicea, Milestones Toward Majorana-Based Quantum Computing, *Phys. Rev. X* **6**, 031016 (2016).
 - [8] V. Mourik, K. Zuo, S. M. Frolov, S. R. Plissard, E. P. A. M. Bakkers, and L. P. Kouwenhoven, Signatures of majorana fermions in hybrid superconductor-semiconductor nanowire devices, *Science* **336**, 1003 (2012).
 - [9] A. Das, Y. Ronen, Y. Most, Y. Oreg, M. Heiblum, and H. Shtrikman, Zero-bias peaks and splitting in an Al–InAs nanowire topological superconductor as a signature of Majorana fermions, *Nat. Phys.* **8**, 887 (2012).
 - [10] M. T. Deng, C. L. Yu, G. Y. Huang, M. Larsson, P. Caroff, and H. Q. Xu, Anomalous zero-bias conductance peak in a Nb–InSb Nanowire–Nb hybrid device, *Nano Lett.* **12**, 6414 (2012).
 - [11] A. D. K. Finck, D. J. Van Harlingen, P. K. Mohseni, K. Jung, and X. Li, Anomalous Modulation of a Zero-Bias Peak in a Hybrid Nanowire-Superconductor Device, *Phys. Rev. Lett.* **110**, 126406 (2013).
 - [12] L. P. Rokhinson, X. Liu, and J. K. Furdyna, The fractional a.c. Josephson effect in a semiconductor–superconductor nanowire as a signature of Majorana particles, *Nat. Phys.* **8**, 795 (2012).
 - [13] M. T. Deng, S. Vaitieknas, E. B. Hansen, J. Danon, M. Leijnse, K. Flensberg, J. Nygård, P. Krogstrup, and C. M. Marcus, Majorana bound state in a coupled quantum-dot hybrid-nanowire system, *Science* **354**, 1557 (2016).
 - [14] S. M. Albrecht, A. P. Higginbotham, M. Madsen, F. Kuemmeth, T. S. Jespersen, J. Nygård, P. Krogstrup, and C. M. Marcus, Exponential protection of zero modes in Majorana islands, *Nature (London)* **531**, 206 (2016).
 - [15] J. Chen, P. Yu, J. Stenger, M. Hocevar, D. Car, S. R. Plissard, E. P. A. M. Bakkers, T. D. Stanescu, and S. M. Frolov, Experimental phase diagram of zero-bias conductance peaks in superconductor/semiconductor nanowire devices, *Sci. Adv.* **3**, e1701476 (2017).
 - [16] H. Zhang, Ö. Gül, S. Conesa-Boj, M. P. Nowak, M. Wimmer, K. Zuo, V. Mourik, F. K. de Vries, J. van Veen, M. W. A. de Moor, J. D. S. Bommer, D. J. van Woerkom, D. Car, S. R. Plissard, E. P. A. M. Bakkers, M. Quintero-Pérez, M. C. Cassidy, S. Koelling, S. Goswami, K. Watanabe, *et al.*, Ballistic superconductivity in semiconductor nanowires, *Nat. Commun.* **8**, 16025 (2017).
 - [17] A. Fornieri, A. M. Whiticar, F. Setiawan, E. Portolés, A. C. C. Drachmann, A. Keselman, S. Gronin, C. Thomas, T. Wang, R. Kallaher, G. C. Gardner, E. Berg, M. J. Manfra, A. Stern, C. M. Marcus, and F. Nichele, Evidence of topological superconductivity in planar Josephson junctions, *Nature (London)* **569**, 89 (2019).
 - [18] H. Ren, F. Pientka, S. Hart, A. T. Pierce, M. Kosowsky, L. Lunczer, R. Schlereth, B. Scharf, E. M. Hankiewicz, L. W. Molenkamp, B. I. Halperin, and A. Yacoby, Topological superconductivity in a phase-controlled Josephson junction, *Nature (London)* **569**, 93 (2019).
 - [19] S. Nadj-Perge, I. K. Drozdov, J. Li, H. Chen, S. Jeon, J. Seo, A. H. MacDonald, B. A. Bernevig, and A. Yazdani, Observation of majorana fermions in ferromagnetic atomic chains on a superconductor, *Science* **346**, 602 (2014).

- [20] S. Jeon, Y. Xie, J. Li, Z. Wang, B. A. Bernevig, and A. Yazdani, Distinguishing a Majorana zero mode using spin-resolved measurements, *Science* **358**, 772 (2017).
- [21] H. Kim, A. Palacio-Morales, T. Posske, L. Rózsa, K. Palotás, L. Szunyogh, M. Thorwart, and R. Wiesendanger, Toward tailoring Majorana bound states in artificially constructed magnetic atom chains on elemental superconductors, *Sci. Adv.* **4**, eaar5251 (2018).
- [22] J.-P. Xu, M.-X. Wang, Z. L. Liu, J.-F. Ge, X. Yang, C. Liu, Z. A. Xu, D. Guan, C. L. Gao, D. Qian, Y. Liu, Q.-H. Wang, F.-C. Zhang, Q.-K. Xue, and J.-F. Jia, Experimental Detection of a Majorana Mode in the Core of a Magnetic Vortex Inside a Topological Insulator-Superconductor $\text{Bi}_2\text{Te}_3/\text{NbSe}_2$ Heterostructure, *Phys. Rev. Lett.* **114**, 017001 (2015).
- [23] H.-H. Sun, K.-W. Zhang, L.-H. Hu, C. Li, G.-Y. Wang, H.-Y. Ma, Z.-A. Xu, C.-L. Gao, D.-D. Guan, Y.-Y. Li, C. Liu, D. Qian, Y. Zhou, L. Fu, S.-C. Li, F.-C. Zhang, and J.-F. Jia, Majorana Zero Mode Detected with Spin Selective Andreev Reflection in the Vortex of a Topological Superconductor, *Phys. Rev. Lett.* **116**, 257003 (2016).
- [24] B. Jäck, Y. Xie, J. Li, S. Jeon, B. A. Bernevig, and A. Yazdani, Observation of a Majorana zero mode in a topologically protected edge channel, *Science* **364**, 1255 (2019).
- [25] P. Zhang, K. Yaji, T. Hashimoto, Y. Ota, T. Kondo, K. Okazaki, Z. Wang, J. Wen, G. D. Gu, H. Ding, *et al.*, Observation of topological superconductivity on the surface of an iron-based superconductor, *Science* **360**, 182 (2018).
- [26] D. Wang, L. Kong, P. Fan, H. Chen, S. Zhu, W. Liu, L. Cao, Y. Sun, S. Du, J. Schneeloch, *et al.*, Evidence for Majorana bound states in an iron-based superconductor, *Science* **362**, 333 (2018).
- [27] Q. Liu, C. Chen, T. Zhang, R. Peng, Y.-J. Yan, C.-H.-P. Wen, X. Lou, Y.-L. Huang, J.-P. Tian, X.-L. Dong, G.-W. Wang, W.-C. Bao, Q.-H. Wang, Z.-P. Yin, Z.-X. Zhao, and D.-L. Feng, Robust and Clean Majorana Zero Mode in the Vortex Core of High-Temperature Superconductor $(\text{Li}_{0.84}\text{Fe}_{0.16})\text{OHFeSe}$, *Phys. Rev. X* **8**, 041056 (2018).
- [28] W. A. Benalcazar, B. A. Bernevig, and T. L. Hughes, Quantized electric multipole insulators, *Science* **357**, 61 (2017).
- [29] F. Schindler, A. M. Cook, M. G. Vergniory, Z. Wang, S. S. P. Parkin, B. A. Bernevig, and T. Neupert, Higher-order topological insulators, *Sci. Adv.* **4**, eaat0346 (2018).
- [30] Z. Song, Z. Fang, and C. Fang, $(d-2)$ -Dimensional Edge States of Rotation Symmetry Protected Topological States, *Phys. Rev. Lett.* **119**, 246402 (2017).
- [31] J. Langbehn, Y. Peng, L. Trifunovic, F. von Oppen, and P. W. Brouwer, Reflection-Symmetric Second-Order Topological Insulators and Superconductors, *Phys. Rev. Lett.* **119**, 246401 (2017).
- [32] E. Khalaf, Higher-order topological insulators and superconductors protected by inversion symmetry, *Phys. Rev. B* **97**, 205136 (2018).
- [33] M. Geier, L. Trifunovic, M. Hoskam, and P. W. Brouwer, Second-order topological insulators and superconductors with an order-two crystalline symmetry, *Phys. Rev. B* **97**, 205135 (2018).
- [34] Z. Yan, F. Song, and Z. Wang, Majorana Corner Modes in a High-Temperature Platform, *Phys. Rev. Lett.* **121**, 096803 (2018).
- [35] Q. Wang, C.-C. Liu, Y.-M. Lu, and F. Zhang, High-Temperature Majorana Corner States, *Phys. Rev. Lett.* **121**, 186801 (2018).
- [36] T. Liu, J. J. He, and F. Nori, Majorana corner states in a two-dimensional magnetic topological insulator on a high-temperature superconductor, *Phys. Rev. B* **98**, 245413 (2018).
- [37] C.-H. Hsu, P. Stano, J. Klinovaja, and D. Loss, Majorana Kramers Pairs in Higher-Order Topological Insulators, *Phys. Rev. Lett.* **121**, 196801 (2018).
- [38] Y. Volpez, D. Loss, and J. Klinovaja, Second-Order Topological Superconductivity in π -Junction Rashba Layers, *Phys. Rev. Lett.* **122**, 126402 (2019).
- [39] X.-H. Pan, K.-J. Yang, L. Chen, G. Xu, C.-X. Liu, and X. Liu, Lattice-Symmetry-Assisted Second-Order Topological Superconductors and Majorana Patterns, *Phys. Rev. Lett.* **123**, 156801 (2019).
- [40] R.-X. Zhang, W. S. Cole, X. Wu, and S. Das Sarma, Higher-Order Topology and Nodal Topological Superconductivity in $\text{Fe}(\text{Se},\text{Te})$ Heterostructures, *Phys. Rev. Lett.* **123**, 167001 (2019).
- [41] M. Kheirkhah, Y. Nagai, C. Chen, and F. Marsiglio, Majorana corner flat bands in two-dimensional second-order topological superconductors, *Phys. Rev. B* **101**, 104502 (2020).
- [42] K. Laubscher, D. Chughtai, D. Loss, and J. Klinovaja, Kramers pairs of Majorana corner states in a topological insulator bilayer, *Phys. Rev. B* **102**, 195401 (2020).
- [43] Y.-X. Li and T. Zhou, Rotational symmetry breaking and partial Majorana corner states in a heterostructure based on high- T_c superconductors, *Phys. Rev. B* **103**, 024517 (2021).
- [44] Z. Yan, Majorana corner and hinge modes in second-order topological insulator/superconductor heterostructures, *Phys. Rev. B* **100**, 205406 (2019).
- [45] Y.-J. Wu, J. Hou, Y.-M. Li, X.-W. Luo, X. Shi, and C. Zhang, In-Plane Zeeman-Field-Induced Majorana Corner and Hinge Modes in an s -Wave Superconductor Heterostructure, *Phys. Rev. Lett.* **124**, 227001 (2020).
- [46] B.-X. Li and Z. Yan, Boundary topological superconductors, *Phys. Rev. B* **103**, 064512 (2021).
- [47] X. Wu, W. A. Benalcazar, Y. Li, R. Thomale, C.-X. Liu, and J. Hu, Boundary-Obstructed Topological High- t_c Superconductivity in Iron Pnictides, *Phys. Rev. X* **10**, 041014 (2020).
- [48] X. Wu, X. Liu, R. Thomale, and C.-X. Liu, High- T_c superconductor $\text{Fe}(\text{Se},\text{Te})$ monolayer: An intrinsic, scalable and electrically tunable Majorana platform, *Natl. Sci. Rev.* **9**, nwab087 (2022).
- [49] X. Zhu, Tunable Majorana corner states in a two-dimensional second-order topological superconductor induced by magnetic fields, *Phys. Rev. B* **97**, 205134 (2018).
- [50] Y. Wang, M. Lin, and T. L. Hughes, Weak-pairing higher order topological superconductors, *Phys. Rev. B* **98**, 165144 (2018).
- [51] Z. Wu, Z. Yan, and W. Huang, Higher-order topological superconductivity: Possible realization in Fermi gases and Sr_2RuO_4 , *Phys. Rev. B* **99**, 020508(R) (2019).
- [52] Z. Yan, Higher-Order Topological Odd-Parity Superconductors, *Phys. Rev. Lett.* **123**, 177001 (2019).
- [53] J. Ahn and B.-J. Yang, Higher-order topological superconductivity of spin-polarized fermions, *Phys. Rev. Res.* **2**, 012060(R) (2020).

- [54] Y.-T. Hsu, W. S. Cole, R.-X. Zhang, and J. D. Sau, Inversion-Protected Higher-Order Topological Superconductivity in Monolayer WTe_2 , *Phys. Rev. Lett.* **125**, 097001 (2020).
- [55] T. Li, M. Geier, J. Ingham, and H. D. Scammell, Higher-order topological superconductivity from repulsive interactions in kagome and honeycomb systems, *2D Mater.* **9**, 015031 (2022).
- [56] H. D. Scammell, J. Ingham, M. Geier, and T. Li, Intrinsic first- and higher-order topological superconductivity in a doped topological insulator, *Phys. Rev. B* **105**, 195149 (2022).
- [57] X. Zhu, Second-Order Topological Superconductors with Mixed Pairing, *Phys. Rev. Lett.* **122**, 236401 (2019).
- [58] M. Kheirkhah, Z. Yan, Y. Nagai, and F. Marsiglio, First- and Second-Order Topological Superconductivity and Temperature-Driven Topological Phase Transitions in the Extended Hubbard Model with Spin-Orbit Coupling, *Phys. Rev. Lett.* **125**, 017001 (2020).
- [59] S. Franca, D. V. Efremov, and I. C. Fulga, Phase-tunable second-order topological superconductor, *Phys. Rev. B* **100**, 075415 (2019).
- [60] S. Ikegaya, W. B. Rui, D. Manske, and A. P. Schnyder, Tunable Majorana corner modes in noncentrosymmetric superconductors: Tunneling spectroscopy and edge imperfections, *Phys. Rev. Res.* **3**, 023007 (2021).
- [61] D. Vu, R.-X. Zhang, and S. Das Sarma, Time-reversal-invariant C_2 -symmetric higher-order topological superconductors, *Phys. Rev. Res.* **2**, 043223 (2020).
- [62] Y.-B. Wu, G.-C. Guo, Z. Zheng, and X.-B. Zou, Multiorder topological superfluid phase transitions in a two-dimensional optical superlattice, *Phys. Rev. A* **104**, 013306 (2021).
- [63] K. Plekhanov, N. Müller, Y. Volpez, D. M. Kennes, H. Schoeller, D. Loss, and J. Klinovaja, Quadrupole spin polarization as signature of second-order topological superconductors, *Phys. Rev. B* **103**, L041401 (2021).
- [64] A. Chew, Y. Wang, B. A. Bernevig, and Z.-D. Song, Higher-Order Topological Superconductivity in Twisted Bilayer Graphene, *arXiv:2108.05373*.
- [65] Y. Tan, Z.-H. Huang, and X.-J. Liu, Two-particle Berry phase mechanism for Dirac and Majorana Kramers pairs of corner modes, *Phys. Rev. B* **105**, L041105 (2022).
- [66] S.-B. Zhang and B. Trauzettel, Detection of second-order topological superconductors by Josephson junctions, *Phys. Rev. Res.* **2**, 012018(R) (2020).
- [67] S.-B. Zhang, A. Calzona, and B. Trauzettel, All-electrically tunable networks of Majorana bound states, *Phys. Rev. B* **102**, 100503(R) (2020).
- [68] T. E. Pahomi, M. Sigrist, and A. A. Soluyanov, Braiding Majorana corner modes in a second-order topological superconductor, *Phys. Rev. Res.* **2**, 032068(R) (2020).
- [69] R.-X. Zhang, W. S. Cole, and S. Das Sarma, Helical Hinge Majorana Modes in Iron-Based Superconductors, *Phys. Rev. Lett.* **122**, 187001 (2019).
- [70] M. J. Gray, J. Freudenstein, S. Y. F. Zhao, R. O'Connor, S. Jenkins, N. Kumar, M. Hoek, A. Kopec, S. Huh, T. Taniguchi, K. Watanabe, R. Zhong, C. Kim, G. D. Gu, and K. S. Burch, Evidence for helical hinge zero modes in an Fe-based superconductor, *Nano Lett.* **19**, 4890 (2019).
- [71] Y. Peng and Y. Xu, Proximity-induced Majorana hinge modes in antiferromagnetic topological insulators, *Phys. Rev. B* **99**, 195431 (2019).
- [72] M. Kheirkhah, Z. Yan, and F. Marsiglio, Vortex-line topology in iron-based superconductors with and without second-order topology, *Phys. Rev. B* **103**, L140502 (2021).
- [73] X.-J. Luo, X.-H. Pan, and X. Liu, Higher-order topological superconductors based on weak topological insulators, *Phys. Rev. B* **104**, 104510 (2021).
- [74] M. Kheirkhah, Z.-Y. Zhuang, J. Maciejko, and Z. Yan, Surface Bogoliubov-Dirac cones and helical Majorana hinge modes in superconducting Dirac semimetals, *Phys. Rev. B* **105**, 014509 (2022).
- [75] H. Shapourian, Y. Wang, and S. Ryu, Topological crystalline superconductivity and second-order topological superconductivity in nodal-loop materials, *Phys. Rev. B* **97**, 094508 (2018).
- [76] S. A. A. Ghorashi, X. Hu, T. L. Hughes, and E. Rossi, Second-order Dirac superconductors and magnetic field induced Majorana hinge modes, *Phys. Rev. B* **100**, 020509(R) (2019).
- [77] N. Bultinck, B. A. Bernevig, and M. P. Zaletel, Three-dimensional superconductors with hybrid higher-order topology, *Phys. Rev. B* **99**, 125149 (2019).
- [78] B. Roy, Higher-order topological superconductors in \mathcal{P} -, \mathcal{T} -odd quadrupolar Dirac materials, *Phys. Rev. B* **101**, 220506(R) (2020).
- [79] A. Tiwari, A. Jahin, and Y. Wang, Chiral Dirac superconductors: Second-order and boundary-obstructed topology, *Phys. Rev. Res.* **2**, 043300 (2020).
- [80] B. Fu, Z.-A. Hu, C.-A. Li, J. Li, and S.-Q. Shen, Chiral Majorana hinge modes in superconducting Dirac materials, *Phys. Rev. B* **103**, L180504 (2021).
- [81] A. K. Ghosh, T. Nag, and A. Saha, Hierarchy of higher-order topological superconductors in three dimensions, *Phys. Rev. B* **104**, 134508 (2021).
- [82] A. Jahin, A. Tiwari, and Y. Wang, Higher-order topological superconductors from Weyl semimetals, *SciPost Phys.* **12**, 053 (2022).
- [83] C.-K. Chiu, J. C. Y. Teo, A. P. Schnyder, and S. Ryu, Classification of topological quantum matter with symmetries, *Rev. Mod. Phys.* **88**, 035005 (2016).
- [84] L. Yang, A. Principi, and N. R. Walet, Rotating Majorana zero modes in a disk geometry, *Phys. Rev. B* **105**, 085417 (2022).
- [85] S.-B. Zhang, W. B. Rui, A. Calzona, S.-J. Choi, A. P. Schnyder, and B. Trauzettel, Topological and holonomic quantum computation based on second-order topological superconductors, *Phys. Rev. Res.* **2**, 043025 (2020).
- [86] M. F. Lapa, M. Cheng, and Y. Wang, Symmetry-protected gates of Majorana qubits in a high- T_c higher-order topological superconductor platform, *SciPost Phys.* **11**, 086 (2021).
- [87] X.-H. Pan, X.-J. Luo, J.-H. Gao, and X. Liu, Braiding higher-order Majorana corner states through their spin degree of freedom, *Phys. Rev. B* **105**, 195106 (2022).
- [88] M. Z. Hasan and C. L. Kane, *Colloquium*: Topological insulators, *Rev. Mod. Phys.* **82**, 3045 (2010).
- [89] X.-L. Qi and S.-C. Zhang, Topological insulators and superconductors, *Rev. Mod. Phys.* **83**, 1057 (2011).
- [90] L. Fu and C. L. Kane, Superconducting Proximity Effect and Majorana Fermions at the Surface of a Topological Insulator, *Phys. Rev. Lett.* **100**, 096407 (2008).
- [91] L. Fu and C. L. Kane, Josephson current and noise at a superconductor/quantum-spin-Hall-insulator/superconductor junction, *Phys. Rev. B* **79**, 161408(R) (2009).

- [92] S.-Q. Shen, *Topological Insulators: Dirac Equation in Condensed Matters* (Springer Science & Business Media, New York, 2013), Vol. 174.
- [93] See Supplemental Material at <http://link.aps.org/supplemental/10.1103/PhysRevB.106.245418> for the details of the following: (i) the derivation of low-energy boundary Hamiltonians; (ii) d -wave pairing case; (iii) the impact of chemical potential on the boundary topological criterion; (iv) sublattice-sensitive Majorana zero modes in time-reversal symmetry broken systems; (v) manipulating the positions of Majorana zero modes by controlling the local boundary potential; (vi) sublattice-sensitive Majorana Kramers pairs in Lieb lattices.
- [94] R. Jackiw and C. Rebbi, Solitons with fermion number $1/2$, *Phys. Rev. D* **13**, 3398 (1976).
- [95] M. Kheirkhah, D. Zhu, J. Maciejko, and Z. Yan, Corner- and sublattice-sensitive Majorana zero modes on the kagome lattice, *Phys. Rev. B* **106**, 085420 (2022).
- [96] D. Zhu, M. Kheirkhah, and Z. Yan, Sublattice-enriched tunability of bound states in second-order topological insulators and superconductors, [arXiv:2211.10905](https://arxiv.org/abs/2211.10905).
- [97] C. L. Kane and E. J. Mele, Quantum Spin Hall Effect in Graphene, *Phys. Rev. Lett.* **95**, 226801 (2005).
- [98] C. L. Kane and E. J. Mele, Z_2 Topological Order and the Quantum Spin Hall Effect, *Phys. Rev. Lett.* **95**, 146802 (2005).
- [99] A. Haim, E. Berg, K. Flensberg, and Y. Oreg, No-go theorem for a time-reversal invariant topological phase in noninteracting systems coupled to conventional superconductors, *Phys. Rev. B* **94**, 161110(R) (2016).
- [100] F. D. M. Haldane, Model for a Quantum Hall Effect without Landau Levels: Condensed-Matter Realization of the “Parity Anomaly”, *Phys. Rev. Lett.* **61**, 2015 (1988).
- [101] X.-L. Qi, T. L. Hughes, and S.-C. Zhang, Topological invariants for the Fermi surface of a time-reversal-invariant superconductor, *Phys. Rev. B* **81**, 134508 (2010).
- [102] H.-M. Guo and M. Franz, Topological insulator on the kagome lattice, *Phys. Rev. B* **80**, 113102 (2009).
- [103] C. Weeks and M. Franz, Topological insulators on the Lieb and perovskite lattices, *Phys. Rev. B* **82**, 085310 (2010).
- [104] S. N. Kempkes, M. R. Slot, J. J. van den Broeke, P. Capiod, W. A. Benalcazar, D. Vanmaekelbergh, D. Bercioux, I. Swart, and C. Morais Smith, Robust zero-energy modes in an electronic higher-order topological insulator, *Nat. Mater.* **18**, 1292 (2019).
- [105] J. A. Stroscio and D. M. Eigler, Atomic and molecular manipulation with the scanning tunneling microscope, *Science* **254**, 1319 (1991).
- [106] O. Custance, R. Perez, and S. Morita, Atomic force microscopy as a tool for atom manipulation, *Nat. Nanotechnol.* **4**, 803 (2009).